Biophysical Journal, Volume 98

Supporting Material

Down-state Model of the Voltage-sensing Domain of a Potassium Channel

Eric V. Schow, J. Alfredo Freites, Karun Gogna, Stephen H. White, and Douglas J. Tobias

SUPPORTING MATERIAL FOR

Down-state Model of the Voltage-sensing Domain of a Potassium Channel

Eric V. Schow*[†], J. Alfredo Freites[‡¶‖], Karun Gogna[‡], Stephen H. White[¶‖], and Douglas J. Tobias[‡‖]

*Department of Physics and Astronomy; [†]Institute for Genomics and Bioinformatics; [‡]Department of Chemistry; [¶]Department of Physiology and Biophysics; and [‖]Center for Biomembrane Systems, University of California, Irvine, CA

Address correspondence to
Douglas Tobias (dtobias@uci.edu) or Stephen White (shwhite@uci.edu)

Restrained MD simulation.

Our model of the KvAP VSD down state was generated using a restrained all-atom MD simulation in a POPC bilayer in excess water, starting from a configuration obtained from a fully equilibrated MD simulation of the VSD in the up state (1). The biotin-avidin VSD accessibility data of Ruta et al. (2) was used as a set of one-dimensional (1D) position restraints along the TM direction. Ruta et al. used biotinylated cysteine substitutions at many locations throughout KvAP in both the pore domain and the VSD to measure the accessibility of membrane-impermeable avidin to biotin tethers of various lengths in order to map the TM depths of the labeled residues in both the open and closed states of the channel. For the VSD, these measurements provided 36 TM constraints, 18 in S1-S2 and 18 in S3b-S4. These data were incorporated into the simulation as 1D distance-dependent restraint forces applied simultaneously on the α-carbons of the 36 residues (see Fig. 1A). The magnitudes of the applied forces were constant (10 kcal mol^{-1} $Å^{-1}$) for distances greater or equal than 2 Å and harmonic (with a 5 kcal mol^{-1} $Å^{-2}$ force constant) for distances less than 2 Å.

In addition to the biotin-avidin position constraints, we also applied two distance constraints; one between the R117 C_ζ atom and the D62 C_γ and the other between the R123 C_ζ atom and the D72 C_γ atom. Distance-dependent forces were applied to both atoms in each pair (see Fig. 1B); the forces were constant (with a magnitude of 10 kcal $mol^{-1}Å^{-1}$) for inter-atomic distances greater than 6 Å, and harmonic (with a 5 kcal mol^{-1} $Å^{-2}$ force constant) for inter-atomic distances between 4 and 6 Å. These restraints were used to encourage the formation of salt bridges. R117 and R123 are the first and third extracellular arginines in S4 (hereafter referred to as R1 and R3, see Fig. S1) while D62 and D72 correspond to the two highly conserved acidic side chain positions in S2 (Fig. S1). The imposition of these restraints arose from the following experimental observations.

In the *Shaker* channel, the substitution of R1 (R362 in the *Shaker* sequence) with smaller, non-charged, side chains is sufficient to open a cation pore through the VSD in the channel closed state (3). Similarly, an R1H mutation generates a proton pore in the closed state (4). These results suggest that, in the wild-type channel, R1 occludes the cation pore and must therefore reside at the interface between the protein and the extracellular medium. In the R1C *Shaker* mutant, Tombola et al. (3) showed that the addition of the E283D mutation (equivalent to D62 in KvAP) increases the cation current through the VSD several-fold. This position, known to interact with S4 arginines in the activated state (5-7), is accessible to the extracellular medium in both the open and closed states of the channel (5, 8). These results led Tombola et al. (3) to suggest that E283 is involved in a salt-bridge interaction with R1 in the *Shaker* channel resting state.

The organization of the conserved acidic side chains in the crystal structure of the Kv1.2 paddle chimera channel (7) suggests that all the S4 basic residues facing the interior of the VSD in the resting state would be involved in salt bridges, and the biotin-avidin VSD accessibility data of Ruta et al. (2) indicate that the S2 segment does not undergo significant TM motions upon activation. These observations prompted the addition of the second salt-bridge restraint. The specific pairing R3-D72 was suggested by the architecture of the KvAP VSD. Although we are not aware of any direct experimental evidence suggesting the occurrence of this specific salt bridge in the VSD

resting state, it is known that the conserved acidic residues in S2 and S3 modulate the voltage-gating function (9), and neutralizing mutations of the residue equivalent to D72 in *Shaker* (E293) were found to have a profound effect on gating current (10).

The specific form and magnitude of the restraint forces were chosen to reach the targets expediently while maintaining the integrity of the VSD in the lipid bilayer system. Because this implied that the restraints could only have a moderate strength, it was necessary to eliminate two VSD internal salt-bridge interactions (E45-R127 and D62-R133) found to be stable along the up-state MD simulation trajectory (1). This was accomplished by protonating the E45 and D62 side chains in the initial configuration of the restrained simulation. The protons were removed after the system arrived at the target configuration and before starting the unrestrained simulation. In addition, during the course of the restrained simulation, a water connection was formed between the extra- and intracellular water-filled crevices of the VSD. We reasoned that this event could affect the overall VSD architecture and, consequently, performed a re-equilibration of the system following a protocol similar to the one reported in (1) before continuing the restrained simulation.

Membrane electrostatics calculations.

We estimated the effect of the presence of the VSD on the membrane electrostatic potential using linearized Poisson-Boltzmann theory, treating all the system components as linear, isotropic dielectrics under an applied potential difference across the membrane, as previously described (11-13). For a given configuration along the simulation trajectory, the electrostatic potential was calculated over a system consisting of a cuboid region, containing the atomistic configurations of the protein and most of the lipids, embedded in a continuum composed of a semi-infinite planar slab, representing the membrane, between two half-spaces that represent the electrolyte solution (12). The calculations were performed using the PBEQ module of the CHARMM 32a2 software package (14). The linearized Poisson-Boltzmann equation was solved by finite difference, using the successive over-relaxation method, on a 130 Å x 130 Å x 72 Å rectangular grid with 2 grid points per Å. The dimensions of the atomistic region were 64 Å x 64 Å x 70 Å. The continuum slab thickness was set to 32 Å, which is the separation between the maxima of the carbonyl distributions in the atomistic system. A dielectric constant of 2 was assigned to lipids and protein. The solvent dielectric constant was set to 80 and the salt concentration was set to 150 mM. The molecular surface was used to define the atomistic dielectric boundaries using the van der Waals radii from the CHARMM force field (15). The final potential maps were obtained by averaging over 340 configuration snapshots of the down-state simulation and 160 configuration snapshots of the up-state simulation, taken every 100 ps in both cases.

The contribution of each amino acid residue to the gating charge associated with the transition from the down-state to the up-state models was estimated as (11, 12):

$$Q_i = \sum_j q_{ij}\left(\phi^{j,up} - \phi^{j,down}\right)$$

where $\phi^{j,up}$ and $\phi^{j,down}$ refer to the electrostatic potential, expressed as a fraction of the applied potential, at the location of the *j*th atom of residue *i* in the up- or down-state configuration, respectively; q_{ij} is the magnitude of the charge on the *j*th atom of residue *i*; the sum runs over all atoms of residue *i*. The total gating charge is the sum of all the residue contributions.

Comparison to biotin-avidin accessibility data.

The biotin-avidin accessibility assay employed by MacKinnon and coworkers (2, 16) relies on the principle that biotin, tethered to a specific residue, can only be captured by avidin at the lipid bilayer interface. Thus, to verify that our simulation trajectories for both the up and down states conform to the biotin-avidin accessibility data, we assumed that for a biotinylated residue to be accessible to avidin, the position of its Cα atom along the TM direction, measured from the lipid bilayer interface, should be within the effective length of the tether (2). To define the bilayer interfaces for comparison of distances to the Ruta et al. data, we used the mean positions of the lipid carbonyl distributions; -18 and 16 Å from the system center, both with a FWHM of ~6 Å (see Fig. S3). Because the biotin-avidin binding event does not distinguish between conformations of the VSD, we assumed that a given residue would be accessible if the specific effective tether length was within the bounds defined by the minimum and maximum Cα position in either trajectory. The results, shown in Figs. S4 and S5, suggest that, overall, the Cα positions in the equilibrated trajectories are consistent with the biotin-avidin accessibility data.

The biotin-avidin accessibility data for the KvAP VSD indicate that only the voltage-sensor paddle (S3b-S4) and the S4-S5 linker are mobile along the TM direction (2, 16). This allowed Ruta et al. (2) to estimate a range of 29-34 Å for the hydrocarbon core thickness based on accessibility measurements in the S1 and S2 segments and the pore domain (S5 segment). These estimates are in good agreement with the location of the lipid carbonyl group in our simulations (-18 and +16 Å) and can be considered to reflect the thermal disorder in the fluid lipid bilayer. The accessibility results from the simulation and the accessibility experiment do not agree for a small subset of residues (3, 5, and 2 for effective tether lengths of 1 Å, 10 Å, and 17 Å, respectively) even when the width of the carbonyl distributions (FWHM of ~6 Å) is taken into account. However, the assumption that the location of the lipid bilayer interface (i.e., the location of the avidin molecule) and the effective tether length are independent of residue position can introduce enough uncertainty to account for these discrepancies, setting aside issues of force field accuracy or the validity of the biotin-avidin reaction as a reliable assay for accessibility. If, for example, instead of taking the mean of the carbonyl distributions as a measure of the extent of penetration of avidin into the polar region of the lipid bilayer, we take the mean phosphate position, all of the discrepancies in S1 through S3 vanish. On the other hand, discrepancies on S4 follow the opposite trend, i.e., they assume a shorter span for the hydrocarbon core, which is consistent with the notion that the outermost charges in S4 are solvated by the lipid phosphate groups, creating a local distortion of the bilayer (17). In addition, the accessibility results derived from the

simulations may be affected by the absence of the pore domain or the fact that not all of the experimental configurations are sampled within the time scale of the trajectories.

REFERENCES

1. Freites, J. A., D. J. Tobias, and S. H. White. 2006. A voltage-sensor water pore. *Biophys. J.* 91:L90-L92.
2. Ruta, V., J. Chen, and R. MacKinnon. 2005. Calibrated measurement of gating-charge arginine. *Cell* 123:463-475.
3. Tombola, F., M. M. Pathak, and E. Y. Isacoff. 2005. Voltage-sensing arginines in a potassium channel permeate and occlude cation-selective pores. *Neuron* 45:379-388.
4. Starace, D. M., and F. Bezanilla. 2004. A proton pore in a potassium channel voltage sensor reveals a focused electric field. *Nature* 427:548-553.
5. Tiwari-Woodruff, S. K., M. A. Lin, C. T. Schulteis, and D. M. Papazian. 2000. Voltage-dependent structural interactions in the Shaker K^+ channel. *J. Gen. Physiol.* 115:123-138.
6. Jiang, Y. X., A. Lee, J. Y. Chen, V. Ruta, M. Cadene, B. T. Chait, and R. MacKinnon. 2003. X-ray structure of a voltage-dependent K^+ channel. *Nature* 423:33-41.
7. Long, S. B., X. Tao, E. B. Campbell, and R. Mackinnon. 2007. Atomic structure of a voltage-dependent K^+ channel in a lipid membrane-like environment. *Nature* 450:376-382.
8. Larsson, B., O. S. Baker, D. S. Dhillon, and E. Y. Isacoff. 1996. Transmembrane movement of the *Shaker* K+ channel S4. *Neuron* 16:387-397.
9. Planells-Cases, R., A. V. Ferrer-Montiel, C. D. Patten, and M. Montal. 1995. Mutation of conserved negatively charged residues in the S2 and S3 transmembrane segments of a mammalian K^+ channel selectively modulates channel gating. *Proc. Natl. Acad. Sci. U.S.A.* 92:9422-9426.
10. Seoh, S. A., D. Sigg, D. M. Papazian, and F. Bezanilla. 1996. Voltage-sensing residues in the S2 and S4 segments of the Shaker K^+ channel. *Neuron* 16:1159-1167.
11. Roux, B. 1997. Influence of the membrane potential on the free energy of an intrinsic protein. *Biophys. J.* 73:2980-2989.
12. Roux, B. 2008. The membrane potential and its representation by a constant electric field in computer simulations. *Biophys. J.* 95:4205-4216.
13. Grabe, M., H. Lecar, Y. N. Jan, and L. Y. Jan. 2004. A quantitative assessment of models for voltage-dependent gating of ion channels. *Proc. Natl. Acad. Sci. U.S.A.* 101:17640-17645.
14. Brooks, B. R. 2009. CHARMM: The biomolecular simulation program. *J. Comput. Chem.* 30:1545-1614.
15. MacKerell, A. D., Jr., D. Bashford, M. Bellott, R. L. Dunbrack, Jr., J. D. Evanseck, M. J. Field, S. Fischer, J. Gao, H. Guo, S. Ha, D. Joseph-McCarthy, L. Kuchnir, K. Kuczera, F. T. K. Lau, C. Mattos, S. Michnick, T. Ngo, D. T. Nguyen, B. Prodhom, W. E. Reiher, III, B. Roux, M. Schlenkrich, J. C. Smith, R. Stote, J. Straub, M. Watanabe, J. Wiórkiewicz-Kuczera, D. Yin, and M. Karplus. 1998. All-atom empirical potential for molecular modeling and dynamics studies of proteins. *J. Phys. Chem. B* 102:3586-3616.
16. Banerjee, A., and R. MacKinnon. 2008. Inferred motions of the S3a helix during voltage-dependent K^+ channel gating. *J. Mol. Biol.* 381:569-580.

17. Krepkiy, D., M. Mihailescu, J. A. Freites, E. V. Schow, D. L. Worcester, K. Gawrisch, D. J. Tobias, S. H. White, and K. J. Swartz. 2009. Structure and hydration of membranes embedded with voltage-sensing domains. *Nature* 462:473-479.

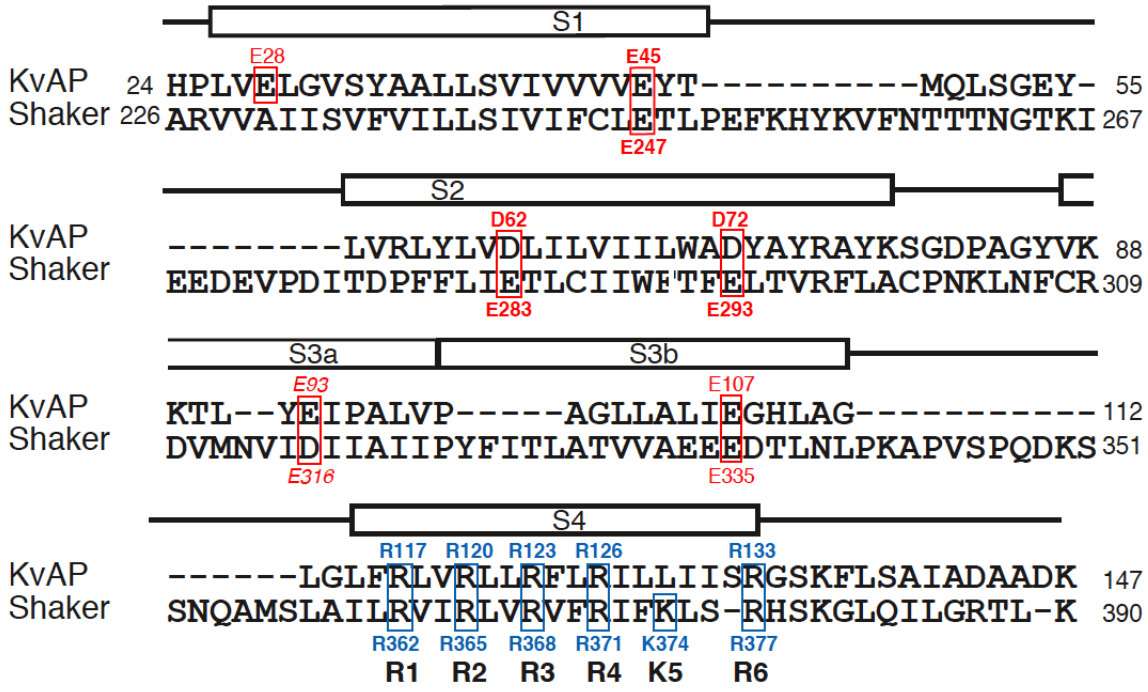

Figure S1. Alignment of the KvAP and *Shaker* VSD domain sequences. Key acidic residues are labeled in red; key basic residues in blue. Those residues that are both highly conserved and participating in salt bridges in our down state model are in bold type; non-conserved residues that participate in down-state salt bridges are in regular type; E93, which is highly conserved but does not participate in a salt bridge is in italics.

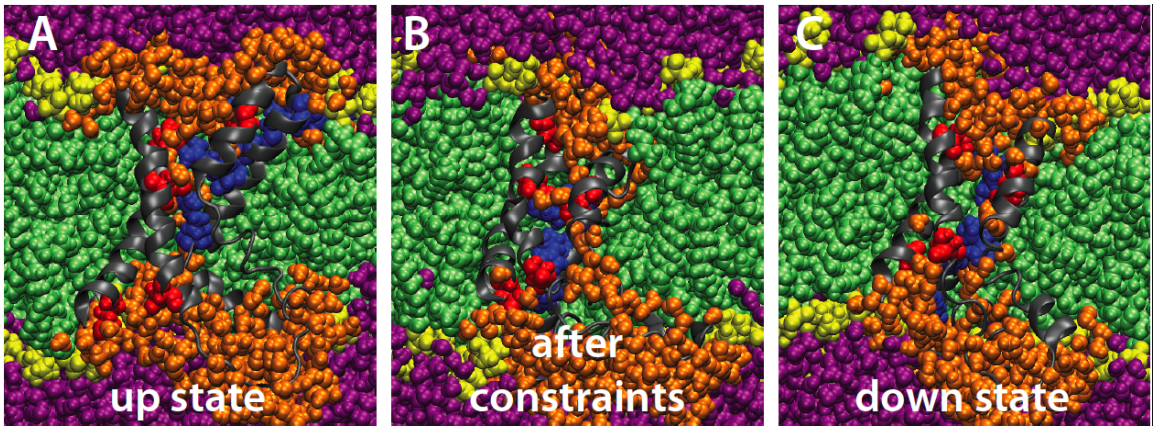

Figure S2: The KvAP VSD in a lipid bilayer at various stages of the model building. The systems are shown in cut-away views. The protein is represented as gray ribbon, with the five S4 arginines in blue space-filling representations, and several key acidic residues shown in red space-filling representations. Lipid head groups are yellow; acyl chains, green; water molecules within 6 Å of the VSD are in orange, and other waters are in purple. (**A**) Snapshot of the equilibrated up state, used as a starting point for the restrained MD simulation. (**B**) The VSD at the end of the restrained simulation phase of the model building. It strictly satisfies the constraints, but the conformation is quite distorted relative to the initial and final states. (**C**) The down-state configuration after 75 ns of unrestrained simulation. The lipid bilayer is distorted around the VSD and water has penetrated the cavities formed by the VSD architecture.

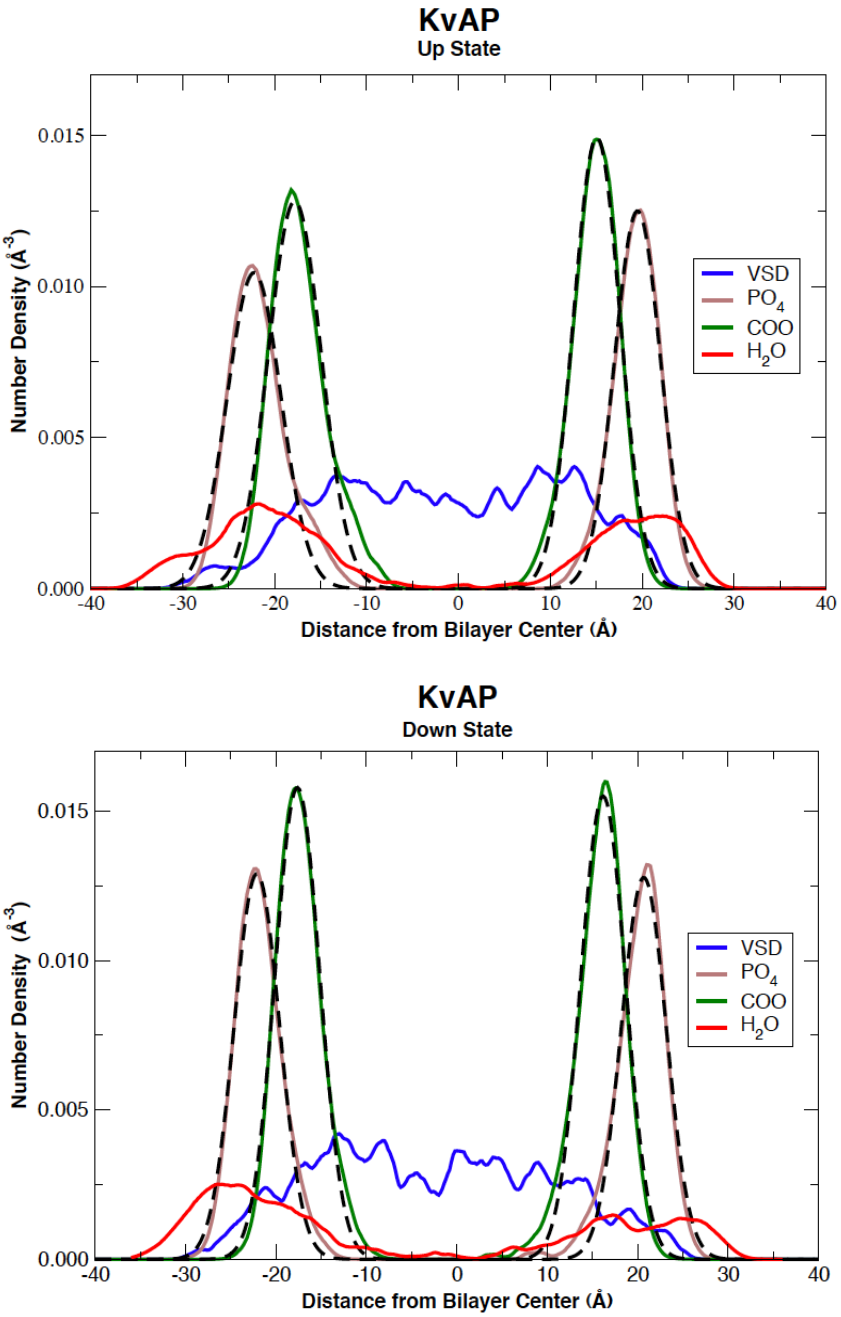

Figure S3. Number density profiles for the VSD, lipid phosphate groups, lipid carbonyl groups, and the water molecules within two solvation shells of the VSD. The phosphate and carbonyl distributions can be modeled as Gaussians (dashed curves) with mean/FWHM of (A) -22.2/3.3 Å and 19.5/2.9 Å (phosphate) and -17.9/3.3 Å and 15.1/2.9 Å (carbonyl) in the up-state simulation. (B) –21.9/3.2 Å and 20.7/2.9 Å (phosphate) and -17.6/2.9 Å and 16.2/2.9 Å (carbonyl) in the down-state simulation. The large inner wings on the phosphate and carbonyl distributions are indicative of interaction between the VSD and lipid groups in the bilayer interior.

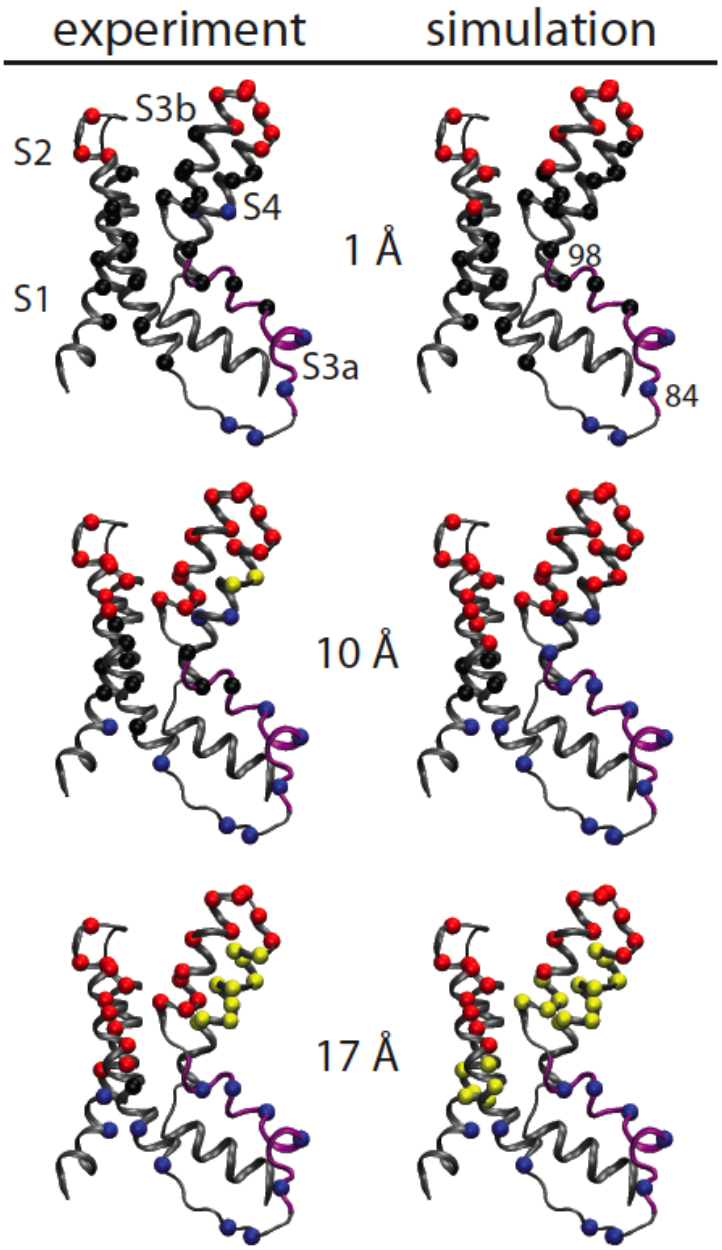

Figure S4. A comparison of biotin-avidin accessibility determined experimentally and by simulation. (**A**) The experimental (left) and simulation (right) results are compared for each effective tether length. Experimental data for residues 84 – 98 in S3a (shown in purple ribbon), were reported in (16) and were not used as 1-D constraints to generate the down-state model. The red spheres correspond to the C_α atoms of biotinylated residues accessible from the extracellular membrane surface, blue spheres to C_α atoms accessible from the intracellular surface, yellow spheres to C_α atoms accessible both extra- and intracellularly. C_α atoms that were completely inaccessible are colored black.

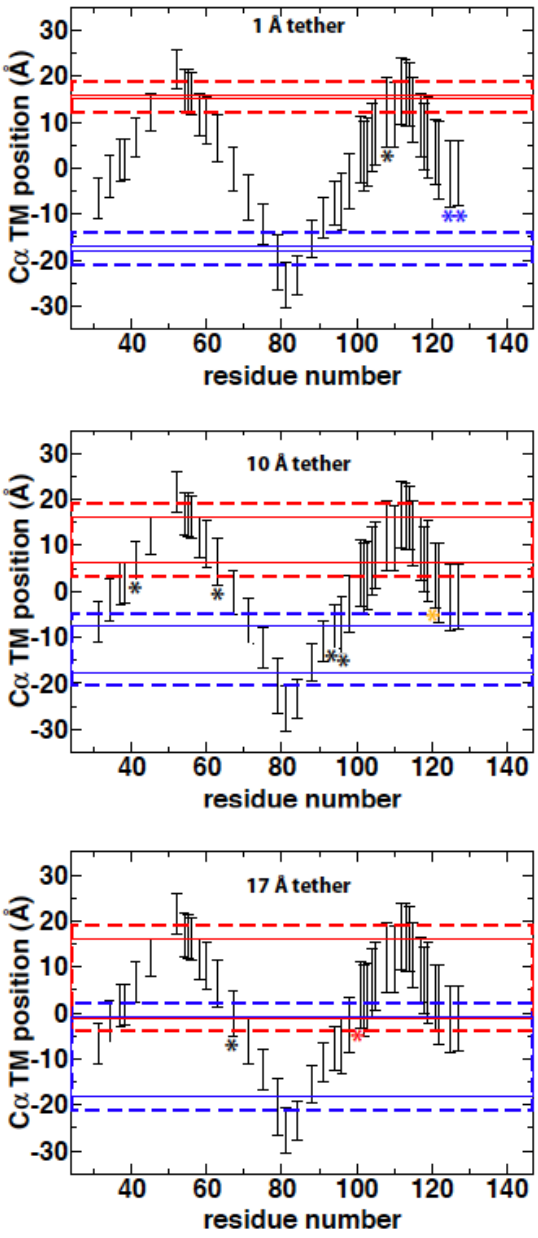

Figure S5. Simulation-based interpretation of biotin-avidin accessibility data (2). The minimum and maximum values of 42 C_α positions along the TM direction are plotted against the effective length of three different biotin tethers. If the C_α range of a given residue falls within the blue or red box the residue is considered to be accessible from the intracellular or the extracellular side, respectively. If the C_α range overlaps both boxes, the residue is considered to be accessible from both sides. The means of the lipid carbonyl distributions (see Fig. S3) determine the outer edge of each box, and the inner edge corresponds to the effective tether length reported by Ruta et al. (2). The dashed lines correspond to half of the carbonyl distribution FWHM. Residues for which the simulation and experimental accessibility results do not agree are labeled with an asterisk. A red asterisk indicates that a residue was experimentally accessible to extracellular avidin; blue, intracellular; yellow, both; and black, inaccessible.

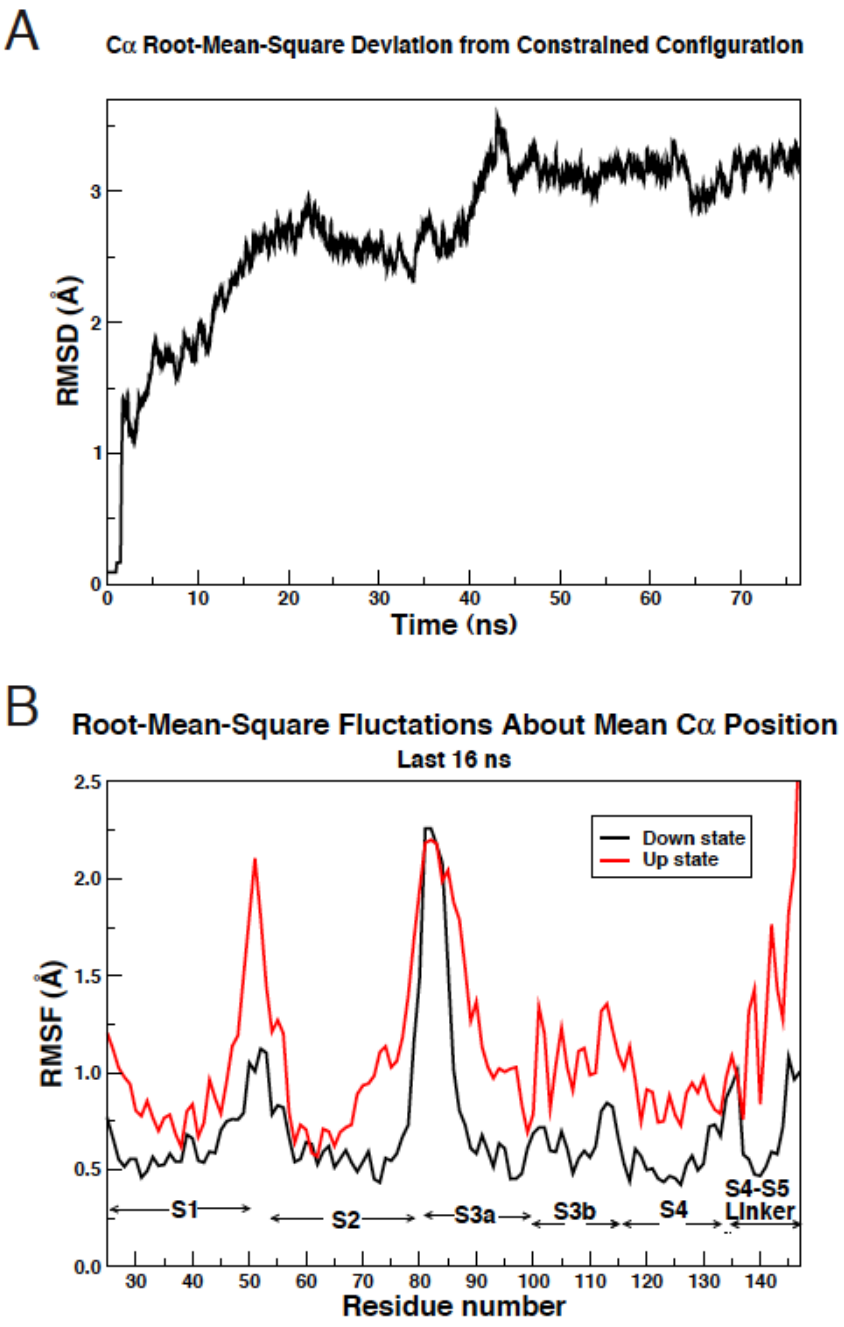

Figure S6. (A) C_α root mean-square deviation (rmsd) from the final constrained configuration. (B) C_α root mean-square fluctuations (rmsf) vs. primary sequence for both simulations.

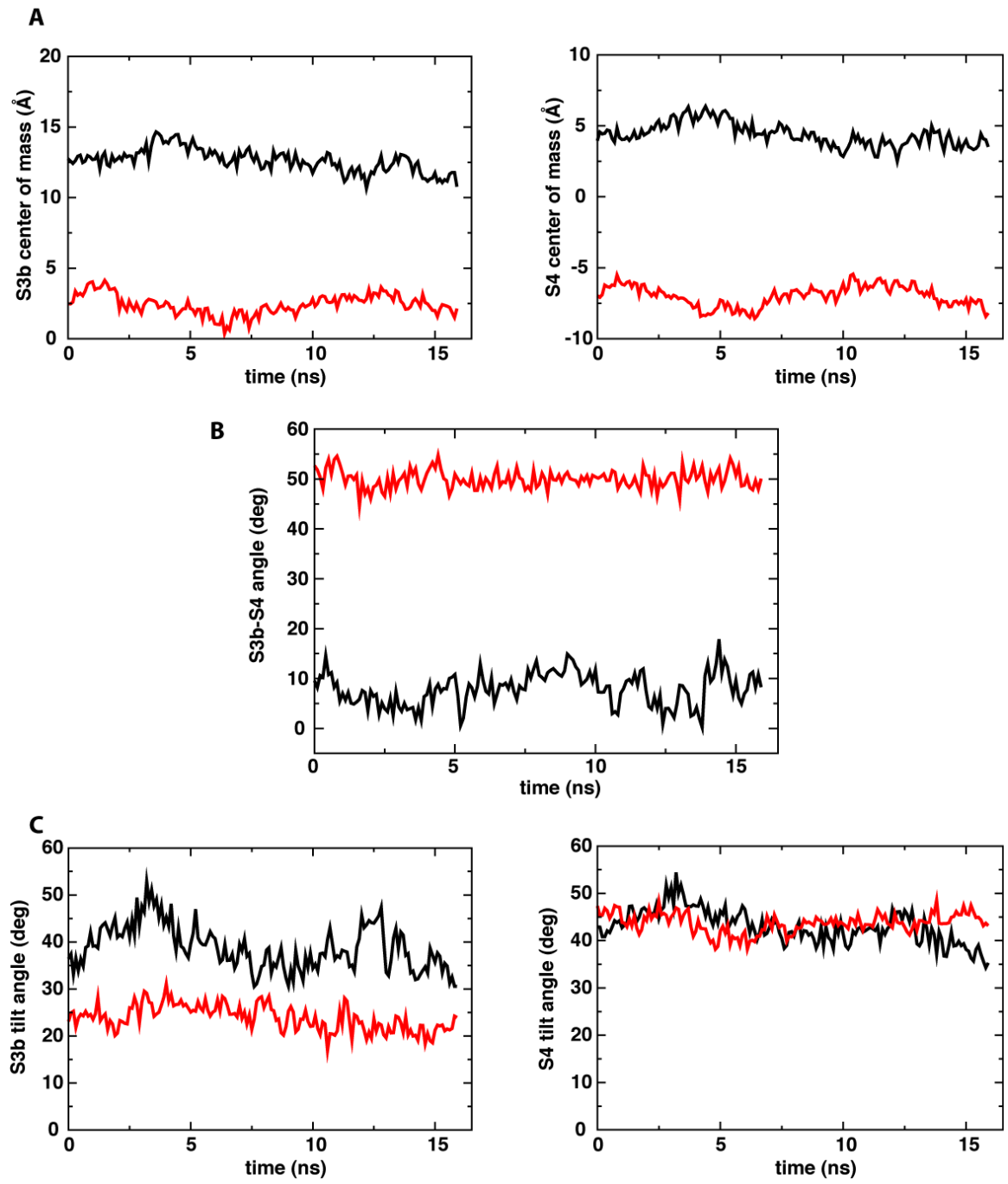

Figure S7. (A) Center-of-mass trajectories for the S3b and S4 segments. (B) Evolution of the angle between S3b and S4. (C) S3b and S4 tilt angle from the TM direction. Red, down-state trajectory; black, up-state trajectory.

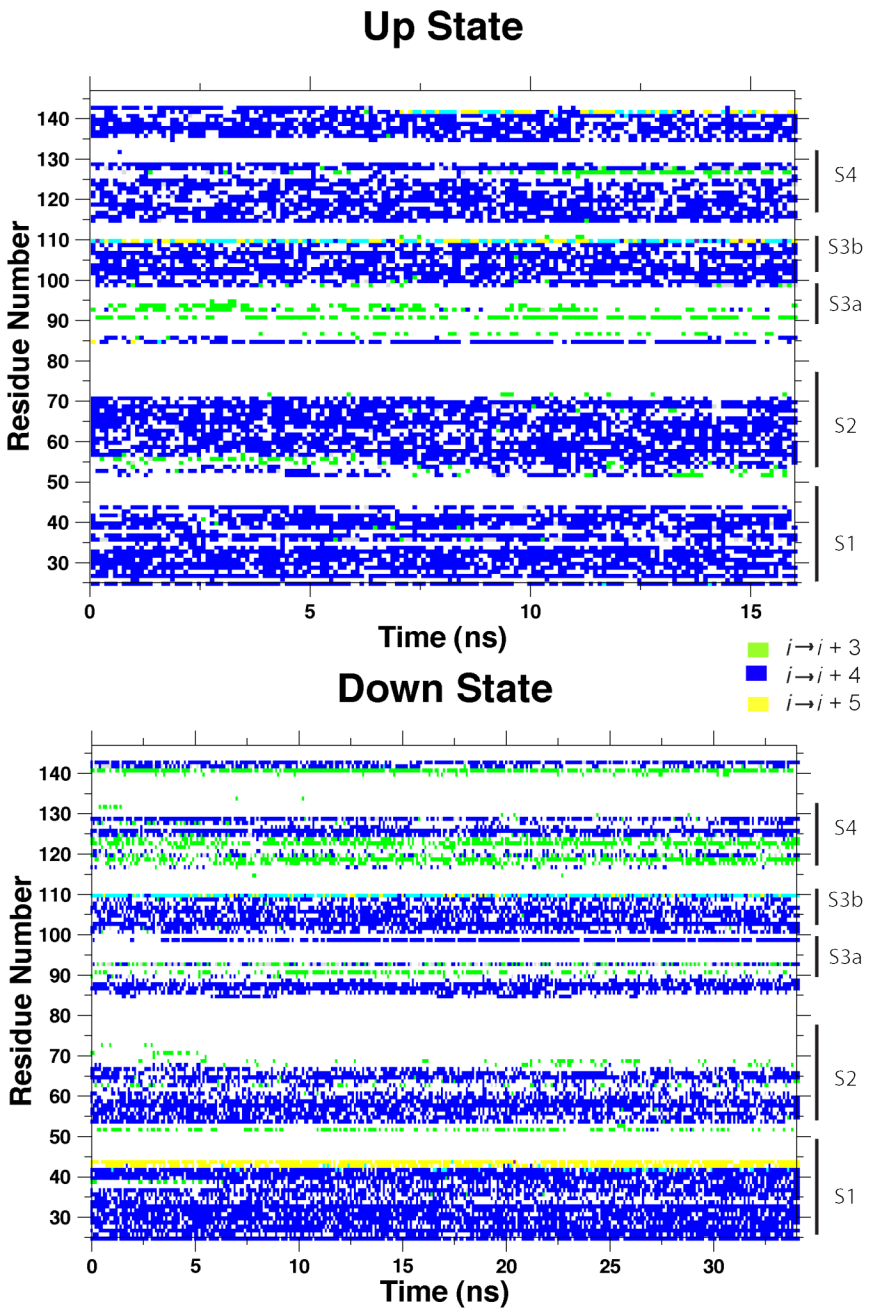

Figure S8. Backbone hydrogen bonding in the KvAP VSD along the equilibrated portion of the up-state trajectory (top), and the down-state trajectory (bottom). A hydrogen bond was considered present when the distance between the donor (backbone oxygen of the i^{th} residue) and acceptor (backbone nitrogen of the $(i + n)^{th}$ residue, where n = 3, 4, or 5) is less than 4 Å, and the donor-hydrogen-acceptor angle ≥ 150°. In the few cases where more than one bond was present, gray indicates $i \rightarrow i+3$ and $i \rightarrow i+4$, and purple indicates $i \rightarrow i+4$ and $i \rightarrow i+5$. The S4 segment exhibits a 3_{10}-helical ($i \rightarrow i+3$ bonding) conformation between V119 and I127.